

This work was written as part of one of the author's official duties as an Employee of the United States Government and is therefore a work of the United States Government. In accordance with 17 U.S.C. 105, no copyright protection is available for such works under U.S. Law.

Public Domain Mark 1.0

<https://creativecommons.org/publicdomain/mark/1.0/>

Access to this work was provided by the University of Maryland, Baltimore County (UMBC) ScholarWorks@UMBC digital repository on the Maryland Shared Open Access (MD-SOAR) platform.

**Please provide feedback**

Please support the ScholarWorks@UMBC repository by emailing [scholarworks-group@umbc.edu](mailto:scholarworks-group@umbc.edu) and telling us what having access to this work means to you and why it's important to you. Thank you.



# An improved pseudo spherical shell algorithm for vector radiative transfer

Peng-Wang Zhai<sup>a,\*</sup>, Yongxiang Hu<sup>b</sup>

<sup>a</sup> Department of Physics, University of Maryland Baltimore County, Maryland, USA

<sup>b</sup> MS 475, NASA Langley Research Center, Hampton, VA 23681-2199, USA

## ARTICLE INFO

### Article history:

Received 29 November 2021

Revised 16 February 2022

Accepted 17 February 2022

Available online 19 February 2022

### Keywords:

Radiative transfer

Spherical shell

## ABSTRACT

The radiative transfer solution in a plane-parallel geometry is a good approximation for many applications in the Earth or other planetary systems as the Earth's radius is quite large ( $\sim 6371$  km). The plane-parallel geometry is however problematic in polar regions where the solar zenith angle is usually large ( $> 60^\circ$ ) and the spherical shell effect is significant. One simple solution is the so-called pseudo-spherical shell (PSS) approximation, which treats the solar beam attenuation exactly along the nadir in the spherical shell atmosphere while keeping the plane parallel geometry for multiple scattering calculation. The PSS approximation improves the solution for intermediately large solar zenith angles, though the error is still large for large viewing zenith angles. In order to further improve the treatment of a spherical shell geometry, we have developed an improved pseudo spherical shell (IPSS) approximation. In the method, we used the following techniques: I.) The single scattering solution is solved exactly for the spherical shell atmosphere; II.) The multiple to single scattering solution ratio is solved using the plane-parallel geometry with our radiative transfer code based on successive order of scattering method; III.) The ratio of the multiple to single scattering solution is assumed to be the same for both the plane parallel and spherical shell geometry. We tested the performance of IPSS with two benchmark cases involving the Rayleigh scattering matrix. If the Rayleigh optical thickness is 0.25, the error is smaller than 1% for most of the viewing directions ( $< 70^\circ$ ). If the Rayleigh optical thickness is 1.0, the error is bounded within  $\pm 2\%$ . The error does not show obvious dependence on the viewing zenith angle. Our newly developed IPSS scheme is highly accurate and can be used in the remote sensing applications of the polar regions.

© 2022 Elsevier Ltd. All rights reserved.

## 1. Introduction

In a most rigorously fashion the radiative transfer solution in the Earth's atmosphere should be solved in a spherical shell geometry [1–5]. As the Earth radius ( $\sim 6371$  km) is quite large comparing to the typical polar-orbiting satellite sensor height ( $\sim 700$  km), it can often be approximated by a plane-parallel geometry in solving the radiative transfer equation for its efficiency and simplicity [6–8]. The plane-parallel solution is problematic for analyzing satellite observations of polar regions where the solar zenith angles are large ( $> 60^\circ$ ) or of limb sounding for which the spherical shell effect is essential. To mitigate the error due to the plane-parallel approximation, a method called the pseudo spherical shell (PSS) model is introduced to the plane-parallel radiative transfer models [9–11], which calculates the attenuation of the solar beam

correctly in the spherical shell geometry from the top of the atmosphere (TOA) to each point along the nadir viewing direction (the green arrow OZ in Fig. 1) [9]. PSS provides the exact single scattering solution to a nadir viewing sensor at TOA. For an oblique view angle the PSS method still shows large errors as the viewing angle increases. Multiple scattering in PSS is calculated in a similar fashion as the plane-parallel geometry.

It has been demonstrated that the PSS method provides accurate radiance at nadir ( $< 0.3\%$ ) for a large range of solar zenith angles (up to  $88^\circ$ ) [9]. However, its error grows larger as both the solar and viewing zenith angles increase. For a viewing zenith angle of  $55^\circ$ , the error of PSS grows from 1% to 10% when the solar zenith angle increase from 0 to  $88^\circ$ , for a typical atmosphere at 317.5 nm. If the solar zenith angle is fixed at  $85^\circ$ , the error due to PSS is in a similar range ( $\pm 10\%$ ), which is larger than the requirements of many remote sensing applications, for example, atmospheric correction of ocean color [12]. Though a number of full spherical radiative transfer codes are available [1–4], it is desir-

\* Corresponding author.

E-mail address: [pwzhai@umbc.edu](mailto:pwzhai@umbc.edu) (P.-W. Zhai).

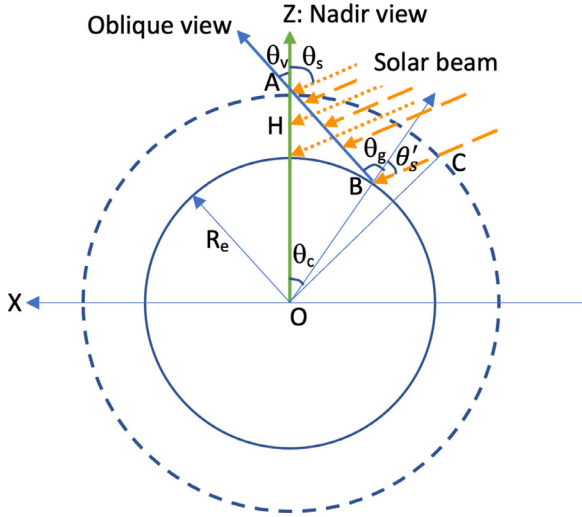


**Fig. 1.** Viewing geometry used in the pseudos-spherical and full spherical simulation.

able to develop a more accurate correction method for applying the plane-parallel based radiative transfer model in the Earth system and retaining the efficiency.

In this paper we report an improved spherical shell correction algorithm (called IPSS hereafter) for radiative transfer solutions in

the plane parallel geometry. The IPSS method includes three key steps: I.) The single scattering solution is rigorously solved in the spherical shell atmosphere; II.) The ratio of the multiple to single scattering solution is solved using the plane-parallel geometry with our radiative transfer code based on the successive order of scattering method [13,14]; III.) The multiple to single scattering ratio is assumed to be the same for the plane parallel and spherical shell geometry, which has been demonstrated by Adams and Kattawar [1] based on their full spherical Monte Carlo code.

The traditional PSS method calculates the attenuation of the solar irradiance in a spherical shell geometry from TOA to an altitude along the nadir viewing direction (see the orange arrows with dot lines along the nadir in Fig. 1). The IPSS solves the exact single scattering solution for which the attenuation of the solar beam at each altitude on a slant path along a non-nadir viewing direction (see the orange arrows with long dash lines along the oblique view in Fig. 1). The error of the PSS approximation increases as the viewing zenith angle increases while the error of the IPSS method does not have obvious dependence on the viewing zenith angle (See Section 3). We implemented both PSS and IPSS to our radiative transfer model based on the successive order of scattering (RTSOS) [13,14], which has been validated against a number of radiative transfer codes, for example, the Matrix Operator method [15] and Markov Chain method [16] presented in [17]. RTSOS naturally provides the radiance field contributions from different orders of scattering, which makes it convenient to calculate the ratio of multiple to single scattering in the plane-parallel geometry. By assuming that the ratio of multiple to single scattering

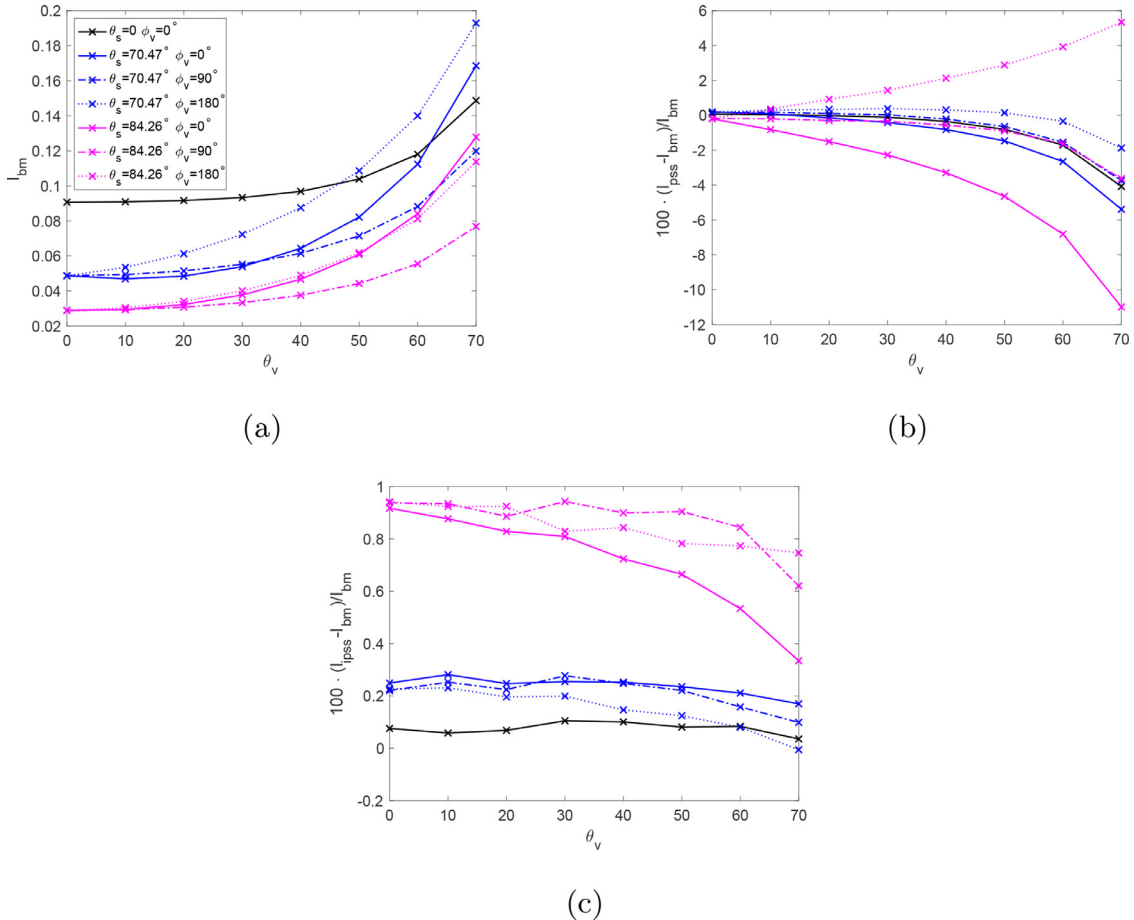


**Fig. 2.** (a) The benchmark radiance  $I_{bm}$  at TOA for a homogeneous Rayleigh atmosphere. The optical thickness is 0.25. The atmosphere is conservative and bounded between 0 and 100 km. The figure legend also applies to Fig. 2b and c. (b) Percentage error of the TOA radiance for PSS with respect to the benchmark. (c) Percentage error of the TOA radiance for IPSS with respect to the benchmark.

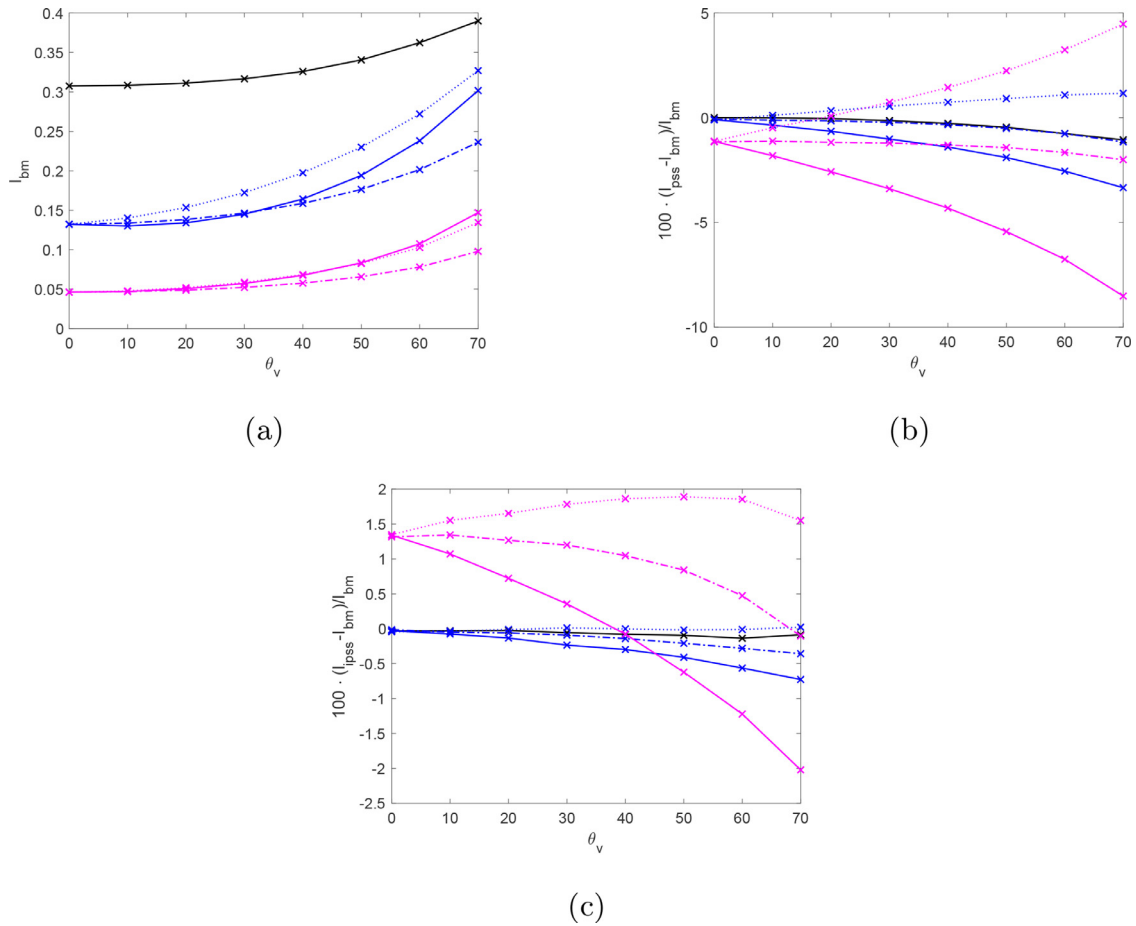


Fig. 3. The same as Fig. 2 but for the optical thickness of 1.0. The figure legend is the same as in Fig. 2a.

contribution is the same in the spherical shell and plane-parallel geometries, we can easily derive the multiple scattering solution based on the exact single scattering solution in spherical shell atmosphere.

We tested the performance of PSS and IPSS based on two cases. One is the benchmark data set for a conservative and homogeneous Rayleigh atmosphere published in [5]. The other is for an inhomogeneous Rayleigh atmosphere with variable single scattering albedo over height [18]. In both cases (homogeneous and inhomogeneous atmospheres) the IPSS results show small errors (<1% if the optical thickness is 0.25 and <2% if the optical thickness is 1.0), which is superior to the PSS method (~10% in similar cases). In addition, the IPSS error shows no obvious dependence on the viewing zenith angle.

In the next Section 2 we describe the algorithm. The simulation results are presented in Section 3. Section 4 is the conclusions.

## 2. Algorithm description

The radiance field is denoted by the Stokes vector  $\mathbf{L} = (I, Q, U, V)^T$ , where I, Q, U, and V are the Stokes parameters; the superscript  $T$  stands for transpose. In the successive order of scattering formulas, the Stokes vector is expressed as a sum of contributions  $\mathbf{L}_n$  from different order of scattering  $n$  [13,14]:

$$\mathbf{L}(\tau, \mu_v, \phi_v) = \sum_{n=1}^N \mathbf{L}_n(\tau, \mu_v, \phi_v), \quad (1)$$

where  $\tau$  is a variable in the unit of optical depth which is used to denote the location of  $\mathbf{L}$ ,  $\mu_v = \cos \theta_v$ ;  $\theta_v$  is the viewing zenith angle;  $\phi_v$  is the viewing azimuth angle;  $\mathbf{L}_n$  is given by an integral form of the radiative transfer equation (see Eq. (6) in [13], which is transformed into a different format below in the context of spherical shell geometry):

$$\mathbf{L}_n(\tau, \mu_v, \phi_v) = \mathbf{L}_n(\tau_b, \mu_v, \phi_v) e^{-\tau_s(\mu_v)} - \int_{\tau_b}^{\tau_s(\mu_v)} e^{-\tau'_s(\mu_v)} \mathbf{S}_n(\tau'_s(\mu_v), \mu_v, \phi_v) d\tau'_s(\mu_v), \quad (2)$$

where  $\tau_s(\mu_v)$  is the slant optical distance along the direction  $\mu_v$  between the boundary (marked by  $\tau_b$  in Eq. (2)) and sensor location  $\tau$ ;  $\mathbf{S}$  is the source vector; and  $\tau'_s(\mu_v)$  is the integration variable along the slant path from the boundary to  $\tau$ .

The source vector  $\mathbf{S}_n$  is given by:

$$\mathbf{S}_1(\tau, \mu_v, \phi_v) = \frac{\omega(\tau)}{4\pi} \mathbf{P}(\tau, \mu_v, \phi_v, \mu_s, \phi_s) [e^{-\tau_s(\mu_s)} \mathbf{E}_0], \quad (3a)$$

$$\mathbf{S}_{n>1}(\tau, \mu_v, \phi_v) = \frac{\omega(\tau)}{4\pi} \int_0^{2\pi} \int_{-1}^1 \mathbf{P}(\tau, \mu_v, \phi_v, \mu', \phi') \cdot \mathbf{L}_{n-1}(\tau, \mu', \phi') d\mu' d\phi', \quad (3b)$$

where  $\mathbf{E}_0 = (E_0, 0, 0, 0)^T$ ;  $E_0$  is the extraterrestrial solar irradiance;  $\omega$  is the single scattering albedo;  $\mathbf{P}$  is the phase matrix of the scattering medium;  $\mu_s = \cos \theta_s$ ;  $\theta_s$  is the solar zenith angle;  $\tau_s(\mu_s)$  is the slant optical distance along the solar beam direction  $\mu_s$  from TOA to location  $\tau$ .

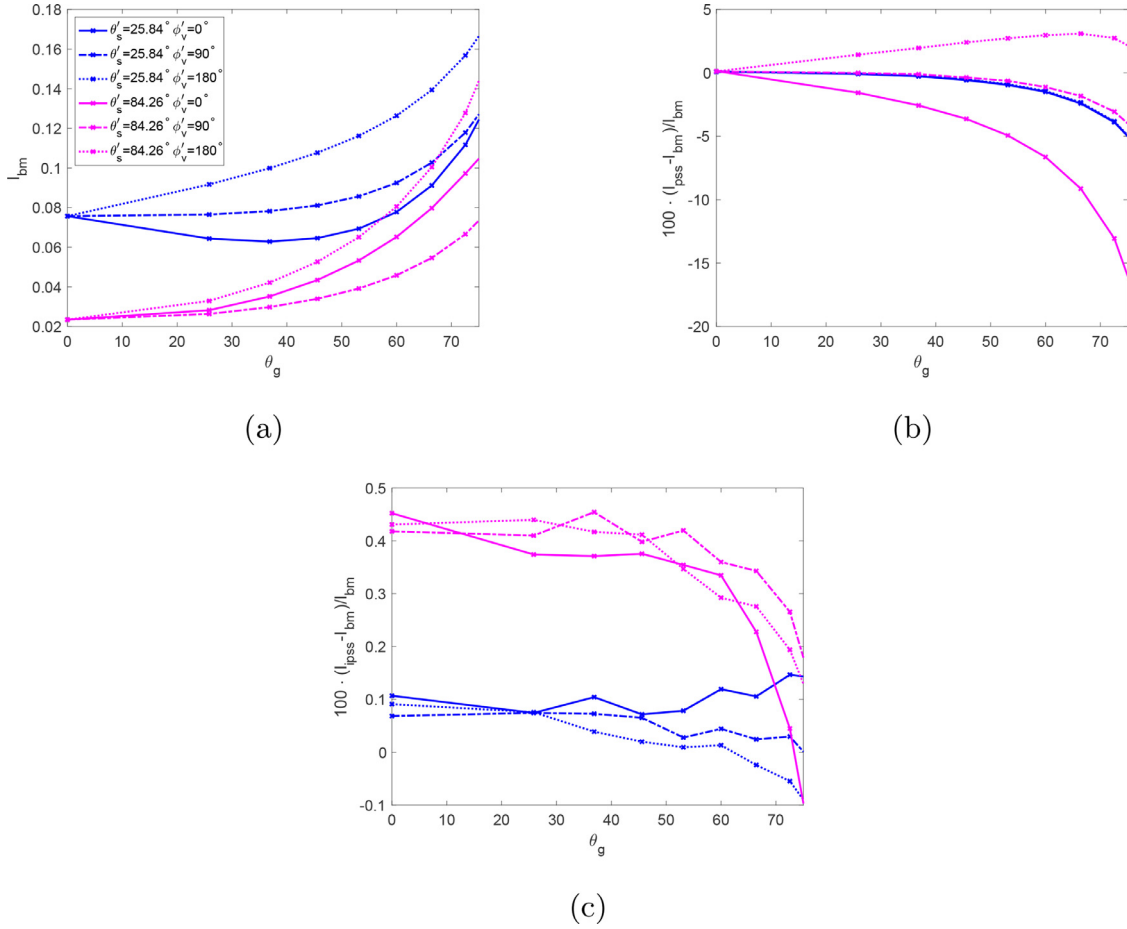


**Fig. 4.** (a) The benchmark radiance  $I_{bm}$  at TOA for an inhomogeneous Rayleigh atmosphere. The optical thickness is 0.25. The atmosphere is bounded between 0 and 100 km. The figure legend also applies to Fig. 4b and c. (b) Percentage error of the TOA radiance for PSS with respect to the benchmark. (c) Percentage error of the TOA radiance for IPSS with respect to the benchmark.

The key difference between the radiative transfer equation in the plane-parallel and spherical shell geometries is the calculation of the slant optical distance  $\tau_s$ . In the plane-parallel geometry,  $\tau_s(\mu_v) = \tau / |\mu_v|$ . In the spherical shell geometry, the calculation of  $\tau_s(\mu_v)$  involves law of sines and cosines in triangles. For example, in a homogeneous atmosphere the slant optical distance along a viewing direction  $\mu_v$  between point A at TOA and point B at the Bottom of the Atmosphere (BOA) (see Fig. 1) can be calculated by:

$$\theta_g = \sin^{-1} \left( \frac{R_e + H}{R_e} \sin \theta_v \right), \quad (4a)$$

$$\theta_c = \theta_g - \theta_v, \quad (4b)$$

$$d = \frac{\sin \theta_c}{\sin \theta_v} R_e, \quad (4c)$$

$$\tau_s(\mu_v) = \beta \cdot d, \quad (4d)$$

where  $R_e$  is the Earth's radius;  $H$  is the TOA height measured from the ground level;  $d$  is the distance between point A and B in Fig. 1;  $\beta$  is the extinction coefficient of the atmosphere. Eqs. (4) and (5)-(6) below can be read as a sort of pseudo-code, i.e., the first line provides necessary inputs to the next line, etc., and the final line is the desired result of the calculation.

To calculate the slant optical depth for an inhomogeneous atmosphere, the atmosphere can be discretized into a set of layers separated by layer height  $h_i$  where  $0 < i < I$  is the height index with  $h_0 = 0$  and  $h_I = H$ . The following equation sequence can be used to find  $\tau_s(\mu_v)$ :

$$\theta' = \sin^{-1} \left( \frac{R_e + H}{R_e + h_i} \sin \theta_v \right), \quad (5a)$$

$$\theta_c = \theta' - \theta_v, \quad (5b)$$

$$d_i = \frac{\sin \theta_c}{\sin \theta_v} R_e, \quad (5c)$$

$$\tau_s(\mu_v) = \sum_{i=1}^I (d_{i-1} - d_i) \cdot \beta_i, \quad (5d)$$

where  $\beta_i$  is the extinction coefficient in layer  $i$ . Eq. (5) can easily be generalized to calculate the slant optical distance from TOA to an arbitrary point of height  $h$  in the atmosphere which is needed to calculate the attenuation of a radiance in the viewing direction of  $\mu_v$  in Eq. (2). Note that  $\tau_s(\mu_v)$  is independent on the viewing azimuth angle  $\phi_v$ .

The single scattering source vector  $\mathbf{S}_1$  in Eq. (3) includes the attenuation term  $e^{-\tau_s(\mu_s)}$ , where  $\tau_s(\mu_s)$  needs to be evaluated from TOA to a point in the atmosphere. In the PSS approximation, this

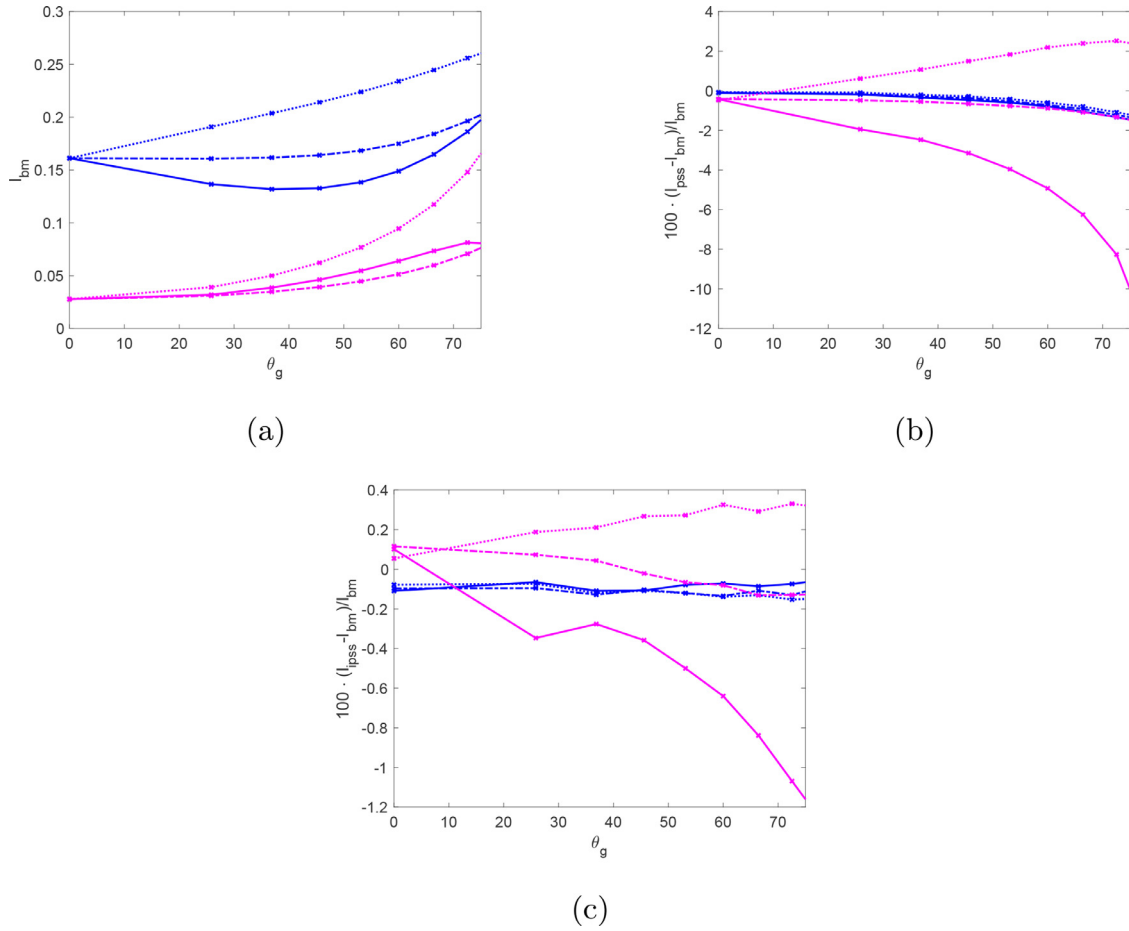


**Fig. 5.** (a) The benchmark radiance  $I_{bm}$  at TOA for an inhomogeneous Rayleigh atmosphere. The optical thickness is 1.0. The atmosphere is bounded between 0 and 100 km. (b) Percentage error of the TOA radiance for PSS with respect to the benchmark. (c) Percentage error of the TOA radiance for IPSS with respect to the benchmark. The figure legend is the same as Fig. 4a.

point is located along the nadir direction (OZ in Fig. 1) [11]. In IPSS, we evaluate the single scattering contribution exactly, so that  $\tau_s(\mu_s)$  is the slant optical distance from TOA to a point along the slant direction AB. This calculation is done in a global coordinate system, of which the z axis is from the center of the Earth O to a sensor located at TOA (OZ in Fig. 1). The x-axis is perpendicular to OZ and in the principal plane which contains the solar beam, and the y-axis is determined by the right hand rule  $\hat{y} = \hat{z} \times \hat{x}$ , where  $\hat{x}$ ,  $\hat{y}$ , and  $\hat{z}$  are the unit vectors along the x, y, and z axes. In this coordinate system the direction of the solar beam is given by  $\mathbf{V}_0 = (\sin \theta_s, 0, -\cos \theta_s)$ . Here as an example we calculate  $\tau_s(\mu_s)$  between point B and C (see Fig. 1) for a homogeneous atmosphere. First the following initializations are made: the coordinates of point A:  $\mathbf{r}_A = (0, 0, R_e + H)$  and the direction vector:  $\mathbf{V} = (\sin \theta_v \cos \phi_v, \sin \theta_v \sin \phi_v, \cos \theta_v)$ . A series of operations can be done in the following sequence:

$$\mathbf{r}_B = \mathbf{r}_A - d \cdot \mathbf{V}, \quad (6a)$$

$$\theta'_s = \cos^{-1} \frac{(\mathbf{r}_B \cdot \mathbf{V}_0)}{|\mathbf{r}_B|}, \quad (6b)$$

$$\angle OCB = \sin^{-1} \left( \frac{\sin \theta'_s}{R_e + H} |\mathbf{r}_B| \right), \quad (6c)$$

$$\angle BOC = \theta'_s - \angle OCB, \quad (6d)$$

$$\delta = \frac{R_e + H}{\sin \theta'_s} \sin \angle BOC, \quad (6e)$$

$$\tau_s(\mu_s) = \beta \cdot \delta, \quad (6f)$$

where  $\mathbf{r}_A$  is the position vector of point A;  $\mathbf{V}$  is the vector representing the viewing direction;  $d$  is the distance between point A and B which can be calculated by Eq. (4c);  $\mathbf{r}_B$  is the position vector of point B;  $|\mathbf{r}_B|$  is the module of vector  $\mathbf{r}_B$  which is the distance from point B to center O;  $\delta$  is the distance from point B to point C. Though A, B, and C in Fig. 1 are placed in the principal plane ( $\phi_v = 0$ ) just for the convenience of annotation, Eq. (6) are indeed applicable to the general situation of  $\phi_v \neq 0$ . For an arbitrary point on AB, Eq. (6) are still applicable if the symbol  $d$  in Eq. (6)(c) is redefined as the distance between point A and the point. For an inhomogeneous atmosphere, Eqs. (6a)–(6f) can be generalized to calculate  $\tau_s(\mu_s)$  in a way similar to Eqs. (5).

With  $\tau_s(\mu_s)$  and  $\tau_s(\mu_v)$  provided by Eqs. (5) and (6), we can evaluate  $\mathbf{S}_1$  in Eq. (3) and consequently  $\mathbf{L}_{1,ss} = (I_{1,ss}, Q_{1,ss}, U_{1,ss}, V_{1,ss})$  from Eq. (2), where the subscript  $ss$  denotes the exact single scattering contribution in the spherical shell geometry. We further introduce  $\mathbf{L}_{pp} = (I_{pp}, Q_{pp}, U_{pp}, V_{pp})$  and  $\mathbf{L}_{1,pp} = (I_{1,pp}, Q_{1,pp}, U_{1,pp}, V_{1,pp})$  as the total Stokes vector and the single scattering solution in the plane-parallel geometry, respectively, which are provided by RTSOS [13,14]. The IPSS method approximates the total Stokes vector  $\mathbf{L}_{ipss} = (I_{ipss}, Q_{ipss}, U_{ipss}, V_{ipss})$  in the

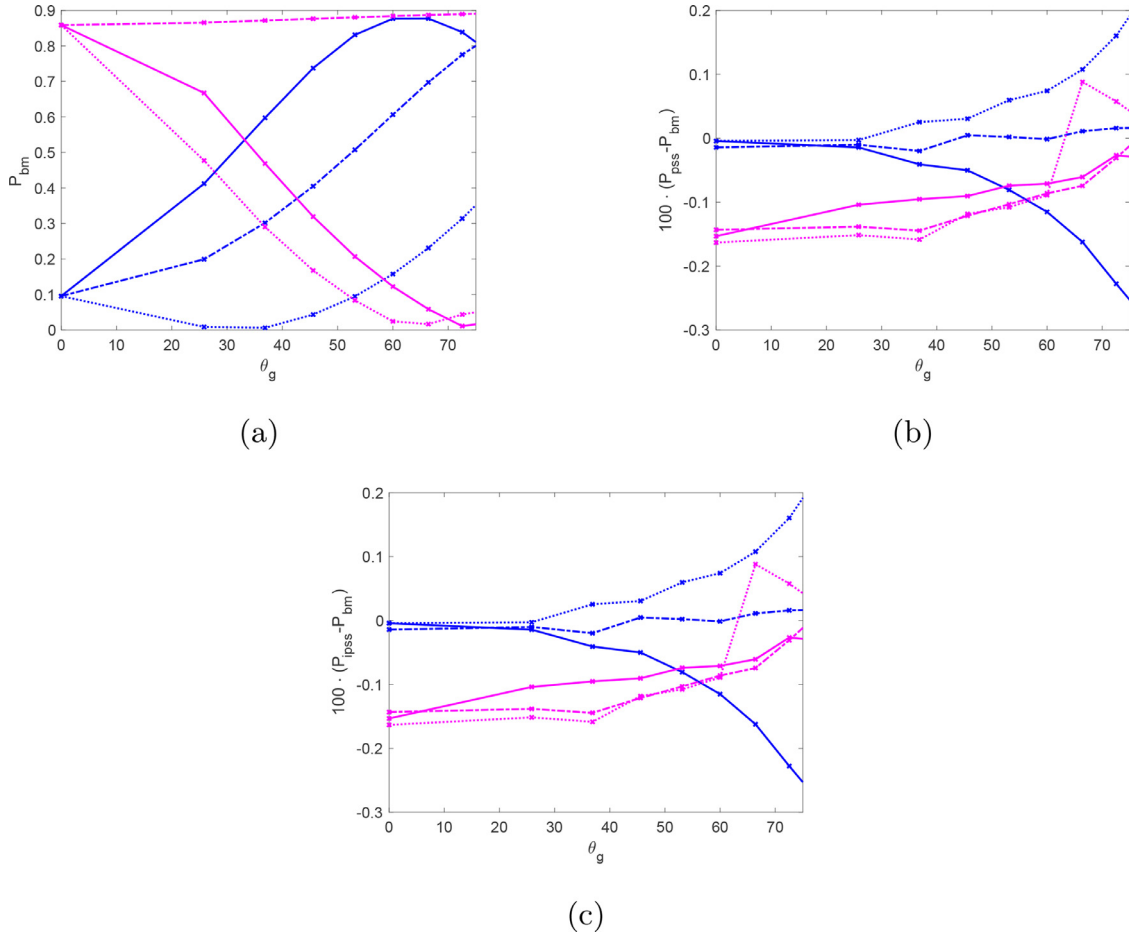


**Fig. 6.** (a) The benchmark degree of linear polarization  $P_{bm}$  at TOA for the same case as in Fig. 4. The optical thickness is 0.25. The atmosphere is bounded between 0 and 100 km. (b) Percentage error of the degree of linear polarization at TOA for PSS with respect to the benchmark. (c) Percentage error of the degree of linear polarization at TOA for IPSS with respect to the benchmark. The figure legend is the same as Fig. 4a.

spherical shell geometry with the equations below:

$$I_{ipss} = \frac{I_{pp}}{I_{1,pp}} I_{1,ss}, \quad (7a)$$

$$Q_{ipss} = \frac{Q_{pp}}{I_{pp}} I_{ipss}, \quad (7b)$$

$$U_{ipss} = \frac{U_{pp}}{I_{pp}} I_{ipss}, \quad (7c)$$

$$V_{ipss} = \frac{V_{pp}}{I_{pp}} I_{ipss}, \quad (7d)$$

where Eq. (7)(a) is the key assumption used in IPSS, which was demonstrated by Adams and Kattawar [1]; and in Eq. (7)(b–d) we assume the ratio of the polarized components (Q, U, and V) to the radiance (I) is the same in spherical shell and the plane parallel geometries, which will be demonstrated later in Section 3

### 3. Validation and performance demonstration

In this section we demonstrate the performance of the IPSS method in two cases. One is the benchmark data set for a homogeneous and conservative Rayleigh atmosphere [5]. The other is for an inhomogeneous atmosphere with variable single scattering albedo [18]. The atmosphere is bounded between 0 and 100 km

for both cases. Two total optical thicknesses  $\tau_t$  are used:  $\tau_t = 0.25$  and  $\tau_t = 1.0$ . For all the results shown below we used a solar irradiance of  $\pi$ . For the first homogeneous case, only scalar radiance is available. In the second inhomogeneous case, full polarization calculation was included, which enables us to check the performance of the approximation in Eq. (7)(b–d).

#### 3.1. Homogeneous atmosphere

In this case, the results are plotted as a function of the viewing zenith angle between 0 and 70° at TOA, which is greater than the scan angles of most satellite sensors. To get the range of the viewing zenith angle  $\theta_g$  at the ground level, we use the law of sines in triangle  $\triangle ABO$  (Eq. (4)(a)) to get  $0 \leq \theta_g \leq 72.64^\circ$  for  $H=100$  km. Fig. 2a show the benchmark radiance  $I_{bm}$  [5] as a function of the viewing zenith angle for the optical thickness of 0.25. Three solar zenith angles: 0°, 70.47°, and 84.26° are shown, which are again defined at TOA. Three viewing azimuth angles 0, 90°, and 180° are included. Fig. 2b shows the percentage error of the PSS method  $\eta_{pss} = 100 \cdot (I_{pss} - I_{bm}) / I_{bm}$ , whereas Fig. 2c shows the percentage error of the IPSS method  $\eta_{ipss} = 100 \cdot (I_{ipss} - I_{bm}) / I_{bm}$ .

For all three solar zenith angles, the PSS error  $\eta_{pss}$  is small ( $<1\%$ ) at the nadir view. However,  $\eta_{pss}$  increases rapidly as the viewing zenith angle increases. For the solar zenith angle of 0°,  $\eta_{pss}$  increases to  $-4\%$  at  $\theta_v = 70^\circ$ . For the non-zero solar zenith angles, the PSS error depends on the viewing azimuth angle. In gen-

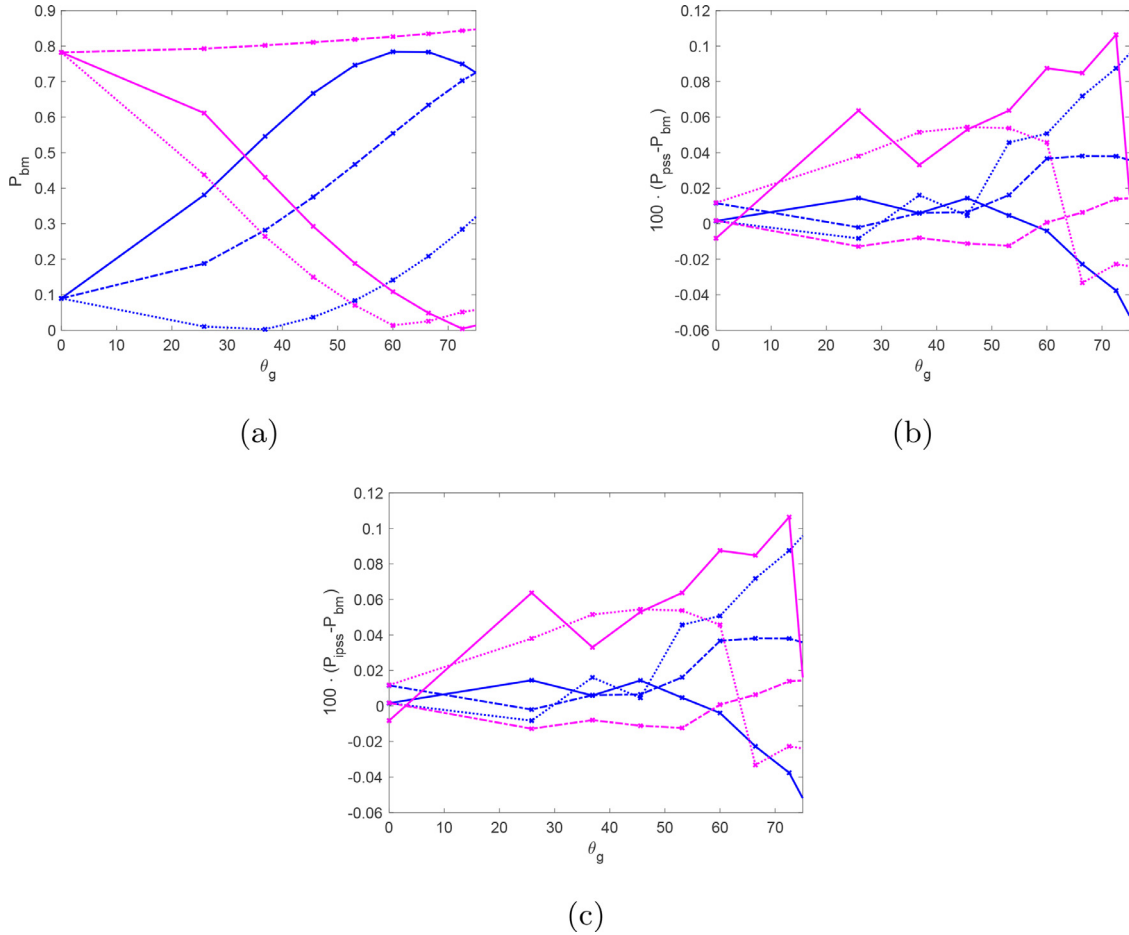


Fig. 7. The same as Fig. 6 except for the optical thickness of 1.0.

eral  $\eta_{pss}$  is largest for  $\phi_v=0$  and smallest for  $\phi_v=180^\circ$ , and the value for  $\phi_v=90^\circ$  is in the middle. For  $\theta_s=70.47^\circ$ ,  $\eta_{pss}$  at  $\theta_v=70^\circ$  is -6%, -4%, and -2% for  $\phi_v=0^\circ, 90^\circ$ , and  $180^\circ$ , respectively. For  $\theta_s=84.26^\circ$ ,  $\eta_{pss}$  at  $\theta_v=70^\circ$  is -11%, -4%, and 5% for  $\phi_v=0^\circ, 90^\circ$ , and  $180^\circ$ , respectively. For the case of IPSS,  $\eta_{ipss}$  is smaller than 1% for all combination of solar and viewing directions. Specifically,  $\eta_{ipss}$  is smaller than 0.1%, 0.3%, 1% for  $\theta_s=0^\circ, 70.47^\circ$ , and  $84.26^\circ$ , respectively. For a small range of viewing zenith angles ( $\theta_v < 10^\circ$ ), the PSS error is smaller than that of IPSS when  $\theta_s=84.26^\circ$ , though the PSS error quickly grow larger as  $\theta_v$  increases. On the other hand,  $\eta_{ipss}$  does not grow as  $\theta_v$  increases which is a great advantage in comparison to the PSS method.

Figs. 3 a–c are the same as Fig. 2a–c except for the optical thickness of  $\tau_t=1.0$ . The range of the PSS error  $\eta_{pss}$  is within (-9%–5%), which is similar to the case of  $\tau_t=0.25$  showing in Fig. 2b. The IPSS error  $\eta_{ipss}$  is within  $\pm 2\%$  for  $\theta_s=84.26^\circ$ , which is higher than the case of  $\tau_t=0.25$ . This is due to the approximation used in Eq. (7)(a) slightly deteriorates for higher optical thickness. However,  $\eta_{ipss}$  remains smaller than  $\eta_{pss}$  and does not increase much as the viewing zenith increases.

### 3.2. Inhomogeneous atmosphere

For the second test case we studied the spherical shell effect for an inhomogeneous atmosphere. Korkin et al. [18] designed this case to include the effect of spherical shell, polarization, and gas absorption in a Rayleigh atmosphere. In this case, the atmosphere is bounded between 0 and 100 km, which is discretized into 100 layers. The thickness of each layer is 1 km. The total optical thick-

ness of the atmosphere is  $\tau_t$ , which is uniformly distributed in each layer. Two values of  $\tau_t$  are chosen, i.e.,  $\tau_t=0.25$  and  $\tau_t=1$ . For each case, the optical thickness of each 1 km layer is  $\tau_t/100$ . The single scattering albedo  $\omega$  of each layer is determined by:

$$\omega = \exp(-\tau) \quad (8)$$

where  $\tau$  is zero at TOA and  $\tau_t$  at BOA. The lower surface is black, i.e., reflection albedo is zero. In each atmospheric layer, the scattering matrix is the Rayleigh scattering matrix with the depolarization ratio of zero. The plane-parallel version of this case was first reported in [19], which is modified in [18] to include spherical shell effects.

Korkin et al. [18] reported highly accurate radiance values at TOA for this inhomogeneous atmosphere based on the comparison of three state-of-the-art radiative transfer codes for spherical shell atmosphere: the MYSTIC code based on the Monte Carlo method [20], the Monte Carlo code for Spherical Shell Atmosphere (MCSSA), and the discrete-ordinate RT code VLIDORT [21]. The MCSSA code was initially written by Adam and Kattawar [1], which has been updated to simulate polarized radiance for sensors at arbitrary locations. The estimation techniques in [22] are implemented in MCSSA to increase efficiency and accuracy. The two Monte Carlo codes (MYSTIC and MCSSA) are exact for the spherical shell atmosphere in a sense that their error decreases as the number of photons increases. The VLIDORT code uses an approximation: multiple scatter spherical correction (VLSC), which applies a spherical shell correction to the plane-parallel simulation. Based on the comparison between MYSTIC and MCSSA, Korkin et al. [18] reported the simulation results for this inhomogeneous atmosphere

with the accuracy within 0.1%, which we will use in the following as the benchmark results. The VLSC method implemented in VLIDORT generates good approximations to the benchmark data, which is within 0–0.7% for the cases studied. For the details of this benchmark data for this inhomogeneous atmosphere, readers are referred to [18].

Different from the case shown in Section 3.1, all angles in this section refers to the values at the bottom of the atmosphere (BOA), which was a discretionary choice of [18]. The benchmark data in [18] included two solar zenith angles  $\theta'_s = \arccos(0.9)$  and  $\arccos(0.1)$ , which are approximately 25.84° and 84.26°, respectively. Three azimuth angles were used:  $\phi'_v = 0^\circ, 90^\circ, 180^\circ$ . Fig. 4a shows the radiance  $I_{bm}$  at TOA for the optical thickness of 0.25 reported in [18] as a function of the viewing zenith angle  $\theta_g$  for two solar zenith angles and three viewing azimuth angles. Fig. 4b shows the percentage error of the radiance calculated by the PSS method in comparison with  $I_{bm}$ , while Fig. 4c is the error for the IPSS method. The PSS error for the inhomogeneous case shows a similar pattern as the homogeneous case, i.e., the error becomes larger as the viewing zenith angle increases. The range of the error is similar to that of the homogeneous case. For the solar zenith angle of 25.84°, the PSS error reaches around -5% at  $\theta_g = 75^\circ$  for all three viewing azimuth angles. For the solar zenith angle of 84.26°, the PSS error at  $\theta_g = 75^\circ$  ranges between -16% ( $\phi'_v = 0^\circ$ ) and 4% ( $\phi'_v = 180^\circ$ ). On the other hand, the IPSS error is much smaller. For the solar zenith angle of 25.84°, the IPSS error is smaller than 0.2% everywhere. For  $\theta'_s = 84.26^\circ$ , the IPSS error is smaller than 0.5%.

Fig. 5 a–c are the same as Fig. 4a–c except for the case of  $\tau_t = 1.0$ . The percentage error of the PSS method is smaller than that of  $\tau_t = 0.25$ , though it is still significant (-10%–3%). The IPSS error is similar to  $\eta_{ipss}$  in Fig. 4c, though the error increases above 1% when  $\theta'_s = 84.26^\circ$ ,  $\phi'_v = 0^\circ$ , and  $\theta_g > 70^\circ$ . Majority of the data falls within 0.5% of the benchmark data reported in [18].

The polarization properties are also important for the remote sensing applications. In Fig. 6a–c we compare the degree of linear polarization

$$P = \sqrt{Q^2 + U^2}/I \quad (9)$$

reported in Korkin et al. [18] and our values calculated from the PSS and IPSS approximations. Fig. 6a shows the benchmark  $P_{bm}$  and Fig. 6b and c show  $100 \cdot (P_{pss} - P_{bm})$  and  $100 \cdot (P_{ipss} - P_{bm})$ , respectively, where the subscripts *pss* and *ipss* indicate the calculation methods. The performance of degree of linear polarization *P* simulated by the PSS and IPSS methods is similar (mostly < 0.3%) in comparing with the benchmark, despite of the fact that PSS generates much larger error in radiance. This confirms that Eq. (7)(b–d) is a useful approximation even in cases where the error of radiance is large. Fig. 7a–c is the same as Fig. 6a–c except for  $\tau_t = 1.0$ . The performance of PSS and IPSS in this case is similar in terms of degree of linear polarization calculation, which is consistent with the case of  $\tau_t = 0.25$ . The errors of  $P_{pss}$  and  $P_{ipss}$  are mostly smaller than 0.1% for this case.

#### 4. Conclusions

In this paper we report an improved pseudo spherical shell (IPSS) correction method for simulating the radiative transfer process in the Earth's polar regions. The method is based on the observation that the ratio of the multiple and single scattering radiances is similar in the plane-parallel and spherical shell geometry, even though the radiance values are drastically different. We calculate this ratio in the plane-parallel geometry by using our radiative transfer model based on the successive order of scattering method, which is combined with the exact single scattering solution in spherical shell geometry to approximate the total radiance field in the spherical shell geometry. The polarization fea-

ture can also be approximated by preserving the ratios ( $Q/I, U/I, V/I$ ) for both the plane-parallel solution and those of the spherical shell case. The method is tested in two cases. One is a homogeneous and conservative Rayleigh atmosphere. The other is an inhomogeneous Rayleigh atmosphere with variable single scattering albedo with height. For both cases, the IPSS method calculates the radiance fairly accurately, with error smaller than 1% for most of the time if the optical thickness is 0.25. The error is within  $\pm 2\%$  if the optical thickness is 1. In addition, the error does not show much dependence on the viewing zenith angle. In the homogeneous case the results discussed are for the viewing zenith angle at TOA smaller than 70°. In the inhomogeneous case the results are shown for the viewing zenith angle at BOA smaller than 75°. In both cases the viewing zenith angle is larger than the scan angle of most satellite sensors. We also showed the results simulated from the traditional pseudo spherical shell (PSS) method, which shows error at the order of -10% – 30% for large solar and viewing zenith angles, which is much larger than the IPSS method. For the two test cases in this study, it takes around 1 sec for a laptop with 2.8 GHz Intel core i-7 CPU to get the plane-parallel radiative transfer solution. The PSS correction barely increase the plane-parallel simulation time, while the IPSS correction takes an extra of 0.05 second. On the other hand, it takes several hours for the backward full-spherical Monte Carlo MCSSA code to finish 100 million photon simulation, which was used to generate the benchmark data used in the inhomogeneous case. This shows the IPSS method is an efficient implementation while keeping a reasonable accuracy, which can be applicable to the remote sensing of environments in the polar regions. The two test cases in this paper involve only the Rayleigh scattering matrix. How the IPSS method performs in atmospheres including aerosols and clouds would be a subject of future studies.

#### Author Statement

PZ was responsible for the conceptualization and methodology of the IPSS method. YH was responsible for the methodology of the PSS and polarization treatment. Both participated in the validation of the code. PZ wrote the original draft and both did writing - review and editing.

#### Declaration of Competing Interest

The authors declare that they have no known competing financial interests or personal relationships that could have appeared to influence the work reported in this paper.

#### Acknowledgments

This research is partially supported by NASA Grants (80NSSC18K0345 and 80NSSC20M0227). We appreciate the discussion with Dr. Bo-Cai Gao at Navel Research Lab, who encouraged us to look into this important subject. The authors also thank Korkin et al. for providing the benchmark data for the inhomogeneous case before it is peer-reviewed.

#### References

- [1] Adams CN, Kattawar GW. Radiative transfer in spherical shell atmospheres: I. Rayleigh scattering. *Icarus* 1978;35(1):139–51. doi:10.1016/0019-1035(78)90067-2.
- [2] Lenoble J, Sekera Z. Equation of radiative transfer in a planetary spherical atmosphere. *Proc Natl Acad Sci* 1961;47(3):372–8. doi:10.1073/pnas.47.3.372.
- [3] Herman BM, Ben-David A, Thome KJ. Numerical technique for solving the radiative transfer equation for a spherical shell atmosphere. *Appl Opt* 1994;33(9):1760–70. doi:10.1364/AO.33.001760.
- [4] Xu F, West RA, Davis AB. A hybrid method for modeling polarized radiative transfer in a spherical-shell planetary atmosphere. *J Quant Spectrosc Radiat Transf* 2013;117:59–70. doi:10.1016/j.jqsrt.2012.10.013.

- [5] Korkin S, Yang E-S, Spurr R, Emde C, Krotkov N, Vasilkov A, Haffner D, Mok J, Lyapustin A. Revised and extended benchmark results for rayleigh scattering of sunlight in spherical atmospheres. *J Quant Spectrosc Radiat Transf* 2020;254:107181. doi:[10.1016/j.jqsrt.2020.107181](https://doi.org/10.1016/j.jqsrt.2020.107181).
- [6] Stamnes K, Tsay S-C, Wiscombe W, Jayaweera K. Numerically stable algorithm for discrete-ordinate-method radiative transfer in multiple scattering and emitting layered media. *Appl Opt* 1988;27(12):2502–9. doi:[10.1364/AO.27.002502](https://doi.org/10.1364/AO.27.002502).
- [7] Jin Z, Charlock TP, Rutledge K, Stamnes K, Wang Y. Analytical solution of radiative transfer in the coupled atmosphere-ocean system with a rough surface. *Appl Opt* 2006;45(28):7443–55. doi:[10.1364/AO.45.007443](https://doi.org/10.1364/AO.45.007443).
- [8] Weng F. A multi-layer discrete-ordinate method for vector radiative transfer in a vertically-inhomogeneous, emitting and scattering atmosphere–I. Theory. *J Quant Spectrosc Radiat Transf* 1992;47(1):19–33. doi:[10.1016/0022-4073\(92\)90076-C](https://doi.org/10.1016/0022-4073(92)90076-C).
- [9] Caudill TR, Flittner DE, Herman BM, Torres O, McPeters RD. Evaluation of the pseudo-spherical approximation for backscattered ultraviolet radiances and ozone retrieval. *J Geophys Res* 1997;102(D3):3881–90. doi:[10.1029/96JD03266](https://doi.org/10.1029/96JD03266).
- [10] Petropavlovskikh I, Loughman R, DeLuise J, Herman B. A comparison of UV intensities calculated by spherical-atmosphere radiation transfer codes: application to the aerosol corrections. *J Geophys Res* 2000;105(D11):14737–46. doi:[10.1029/2000JD900136](https://doi.org/10.1029/2000JD900136).
- [11] He X, Stamnes K, Bai Y, Li W, Wang D. Effects of earth curvature on atmospheric correction for ocean color remote sensing. *Remote Sens Environ* 2018;209:118–33. doi:[10.1016/j.rse.2018.02.042](https://doi.org/10.1016/j.rse.2018.02.042).
- [12] Frouin RJ, Franz BA, Ibrahim A, Knobelspiesse K, Ahmad Z, Cairns B, Chowdhary J, Dierssen HM, Tan J, Dubovik O, Huang X, Davis AB, Kalashnikova O, Thompson DR, Remer LA, Boss E, Coddington O, Deschamps P-Y, Gao B-C, Gross L, Hasekamp O, Omar A, Pelletier B, Ramon D, Steinmetz F, Zhai P-W. Atmospheric correction of satellite ocean-color imagery during the pace era. *Front Earth Sci* 2019;7:145. doi:[10.3389/feart.2019.00145](https://doi.org/10.3389/feart.2019.00145).
- [13] Zhai P-W, Hu Y, Trepte CR, Lucker PL. A vector radiative transfer model for coupled atmosphere and ocean systems based on successive order of scattering method. *Opt Express* 2009;17(4):2057–79. doi:[10.1364/OE.17.002057](https://doi.org/10.1364/OE.17.002057).
- [14] Zhai P-W, Hu Y, Chowdhary J, Trepte CR, Lucker PL, Josset DB. A vector radiative transfer model for coupled atmosphere and ocean systems with a rough interface. *J Quant Spectrosc Radiat Transf* 2010;111(7):1025–40. doi:[10.1016/j.jqsrt.2009.12.005](https://doi.org/10.1016/j.jqsrt.2009.12.005).
- [15] Chowdhary J, Cairns B, Travis LD. Contribution of water-leaving radiances to multiangle, multispectral polarimetric observations over the open ocean: bio-optical model results for case 1 waters. *Appl Opt* 2006;45(22):5542–67. doi:[10.1364/AO.45.005542](https://doi.org/10.1364/AO.45.005542).
- [16] Xu F, Davis AB, West RA, Esposito LW. Markov chain formalism for polarized light transfer in plane-parallel atmospheres, with numerical comparison to the Monte Carlo method. *Opt Express* 2011;19(2):946–67. doi:[10.1364/OE.19.000946](https://doi.org/10.1364/OE.19.000946).
- [17] Chowdhary J, Zhai P-W, Xu F, Frouin R, Ramon D. Testbed results for scalar and vector radiative transfer computations of light in atmosphere-ocean systems. *J Quant Spectrosc Radiat Transf* 2020;242:106717. doi:[10.1016/j.jqsrt.2019.106717](https://doi.org/10.1016/j.jqsrt.2019.106717).
- [18] Korkin S, Yang E-S, Spurr R, Emde C, Zhai P, Krotkov N, Vasilkov A, Lyapustin A. Numerical results for polarized light scattering in a spherical atmosphere. *J Quant Spectrosc Radiat Transf* 2022. Submitted.
- [19] Mishchenko M. The fast invariant imbedding method for polarized light: computational aspects and numerical results for Rayleigh scattering. *J Quant Spectrosc Radiat Transf* 1990;43(2):163–71. doi:[10.1016/0022-4073\(90\)90045-8](https://doi.org/10.1016/0022-4073(90)90045-8).
- [20] Emde C, Buras R, Mayer B. ALIS: an efficient method to compute high spectral resolution polarized solar radiances using the Monte Carlo approach. *J Quant Spectrosc Radiat Transf* 2011;112(10):1622–31. doi:[10.1016/j.jqsrt.2011.03.018](https://doi.org/10.1016/j.jqsrt.2011.03.018).
- [21] Spurr RJ. VLIDORT: a linearized pseudo-spherical vector discrete ordinate radiative transfer code for forward model and retrieval studies in multilayer multiple scattering media. *J Quant Spectrosc Radiat Transf* 2006;102(2):316–42. doi:[10.1016/j.jqsrt.2006.05.005](https://doi.org/10.1016/j.jqsrt.2006.05.005).
- [22] Zhai P-W, Kattawar GW, Yang P. Impulse response solution to the three-dimensional vector radiative transfer equation in atmosphere-ocean systems. I. Monte Carlo method. *Appl Opt* 2008;47(8):1037–47. doi:[10.1364/AO.47.001037](https://doi.org/10.1364/AO.47.001037).